Journal of Pharmaceutical and Biomedical Analysis 48 (2008) 885–896

Contents lists available at ScienceDirect

Journal of Pharmaceutical and Biomedical Analysis

journal homepage: www.elsevier.com/locate/jpba

Structural elucidation of *in vitro* and *in vivo* metabolites of cryptotanshinone by HPLC–DAD–ESI–MS^n

Haixue Dai [1], Mingming Wang [1], Xiaorong Li, Lijuan Wang, Yuhang Li, Ming Xue *

Department of Pharmacology, School of Chemical Biology & Pharmaceutical Sciences, Capital Medical University, Beijing 100069, PR China

ARTICLE INFO

Article history:
Received 7 December 2007
Received in revised form 30 June 2008
Accepted 3 July 2008
Available online 23 July 2008

Keywords:
Structural elucidation
Cryptotanshinone
Metabolites
LC–DAD–ESI–MS^n

ABSTRACT

The structural elucidation of the *in vivo* and *in vitro* metabolites of cryptotanshinone which was the major active component isolated from rhizome of *Salvia miltiorrhiza* Bunge and possessed significant antibacterial, anti-dermatophytic, antioxidant, anti-inflammatory and anticancer activities was described. Nineteen phase I metabolites and six phase II metabolites of cryptotanshinone were elucidated and identified by a sensitive LC–DAD–ESI–MS^n method, and their molecular structures were proposed on the basis of the characteristics of their precursor ions, product ions, chromatographic retention time and ultraviolet spectra. The *in vivo* and *in vitro* phase I metabolites were mainly biotransformed by four main routes, which were dehydrogenation, hydroxylation, furan ring cleavage and oxidation metabolism, and among these phase I reactions, dehydrogenation was the predominant metabolic pathway. Six *in vivo* phase II metabolites were identified as the glucuronided and the sulfated conjugates which showed a neutral loss of 176 and 80 Da, respectively. The biotransformation pathways of cryptotanshinone were proposed on the basis of this research.

1. Introduction

Drug metabolic profile plays an important role in discovering and developing the novel drug from the metabolites possessed the pharmacological activities. The structure profile of the metabolites provides an essential perspective for the synthetic refinement and the candidates among an extensive series of potential structures, resulting in an optimum drug effectiveness and safety.

Traditional Chinese medicine (TCM) has gained ever-increasing popularity in the world because of the therapeutic effects for some serious diseases and these effects are mostly due to the active metabolites from the natural drugs [1]. Therefore, the investigation of the active metabolites from TCM constituents and preparations are of significance in the elucidation of the therapeutic mechanisms. The root of *Salvia miltiorrhiza* Bunge (SMB, named as Danshen in China), a well-known traditional Chinese herbal medicine, has been used extensively for the treatment of coronary heart disease, particularly angina pectoris and myocardial infarction for many years [2,3].

Cryptotanshinone (CT), which is the mainly active component isolated from the root of SMB, has attracted particular attention of chemists and clinicians all over the world due to its powerful and various kinds of pharmacological activities including antibacterial and anti-dermatophytic [4,5], antioxidant [6], anti-inflammatory [7] and anticancer [8] activities. Cryptotanshinone also can inhibit endothelia cells producing endothelin-1 [9] and induce the differentiation of some cells such as bone marrow mesenchymal stem cells [10]. In recent years, investigations on cryptotanshinone were focused on the isolation and purification [11], quantification and pharmacological activates [12,13]. Some investigations [14–18,27,28] have dealt with the metabolism of cryptotanshinone or tanshinones to some extent. In previous work, we reported six phase I metabolites of cryptotanshinone in pigs. Compared the metabolic products of cryptotanshinone, there was some differences in the species metabolism between rat and pig. Some metabolites of cryptotanshinone such as tanshinone IIA, hydroxyltanshinone IIA, etc. were also the chemical components of danshen diterpene quinones which mainly existed in the roots of *S. miltiorrhiza* Bunge and had many pharmacological activities including antibacterial, anti-dermatophytic, antioxidant, anti-inflammatory and anticancer activities. But the study of this drug metabolism is still limited; no report was seen in the literature comparatively detailed with the structural elucidation of *in vivo* and *in vitro* metabolites of cryptotanshinone by power liquid chromatography–diode array detection–electrospray ionization–tandem mass spectrometry (LC–DAD–ESI–MS^n). In this paper, nineteen phase I and six phase II metabolites of cryptotanshinone *in vivo* and *in vitro* were simultaneously elucidated and identified by LC–DAD–ESI–MS^n method. The structures of the

* Corresponding author. Tel.: +86 10 83911520; fax: +86 10 83911520.
E-mail address: xuem@ccmu.edu.cn (M. Xue).
[1] Co-first author.

0731-7085/$ – see front matter © 2008 Elsevier B.V. All rights reserved.
doi:10.1016/j.jpba.2008.07.011

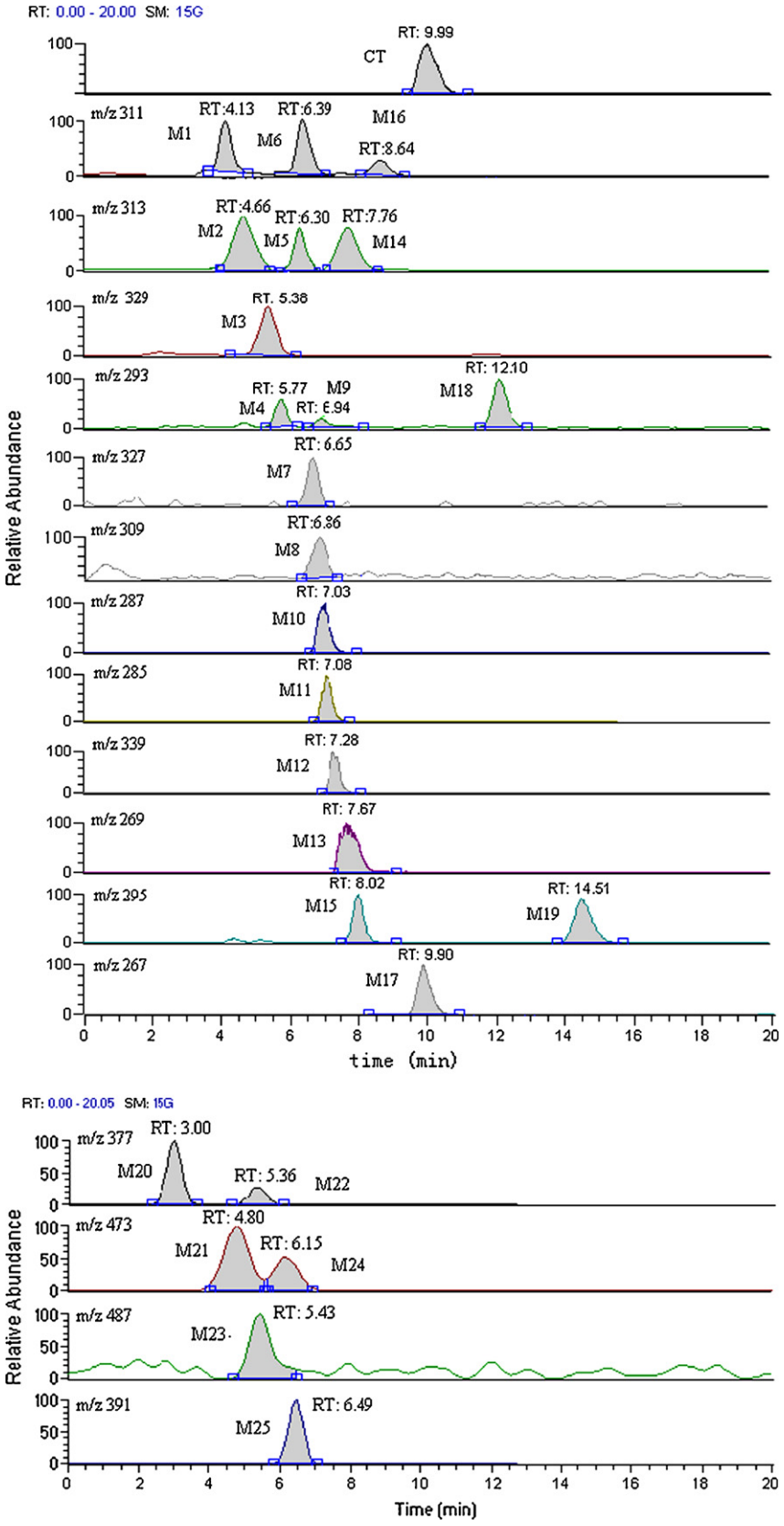

Fig. 1. Extracted ion chromatograms of cryptotanshinone and its phase I and phase II metabolites in rat.

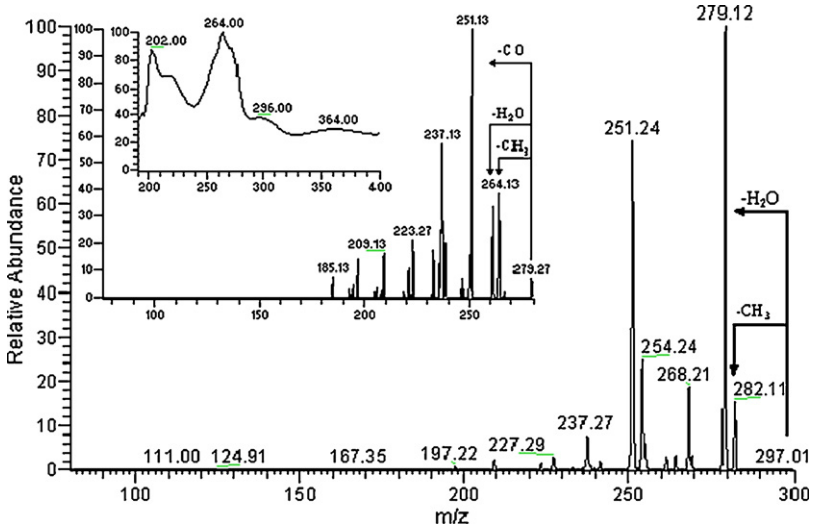

Fig. 2. The MS^2 [297], MS^3 [297 → 279] spectra and UV spectrum of the protonated molecule of cryptotanshinone.

metabolites were characterized on the basis of their precursor ions, product ions, UV spectra, and HPLC retention time. Finally, the biotransformation pathways of cryptotanshinone in rat were elucidated on the basis of *in vitro* and *in vivo* metabolism study. The investigation could help readers in the field to better understand the metabolic mechanism and intermediate process of this compound. The results may provide important data for predicting the metabolic stability, and developing a novel drug or lead compound and better using in the clinical practice.

2. Experimental

2.1. Chemicals and reagents

Cryptotanshinone (mw = 296) was obtained from our laboratory, which was isolated and purified from the root of *S. miltiorrhiza* Bunge and identified as pure compound from the melting point, IR, UV, MS, NMR and compared with the standard compound, the purity of cryptotanshinone was above 99% [19]. The standard compound cryptotanshinone and tanshinone IIA were purchased from the National Institute for the Control of Pharmaceutical and Biological Products (Beijing, China). Methanol used was of HPLC grade and purchased from Fisher Scientific Products (Fair Lawn, NJ, USA). Water was triply distilled. Ethyl acetate and other reagents and solvents used were all of analytical grade.

2.2. In vitro incubation and sample preparation

All studies on animals were in accordance with the guidelines of the Committee on the Care and Use of Laboratory Animals of China. Healthy male Sprague–Dawley rats (210–250 g) were obtained from

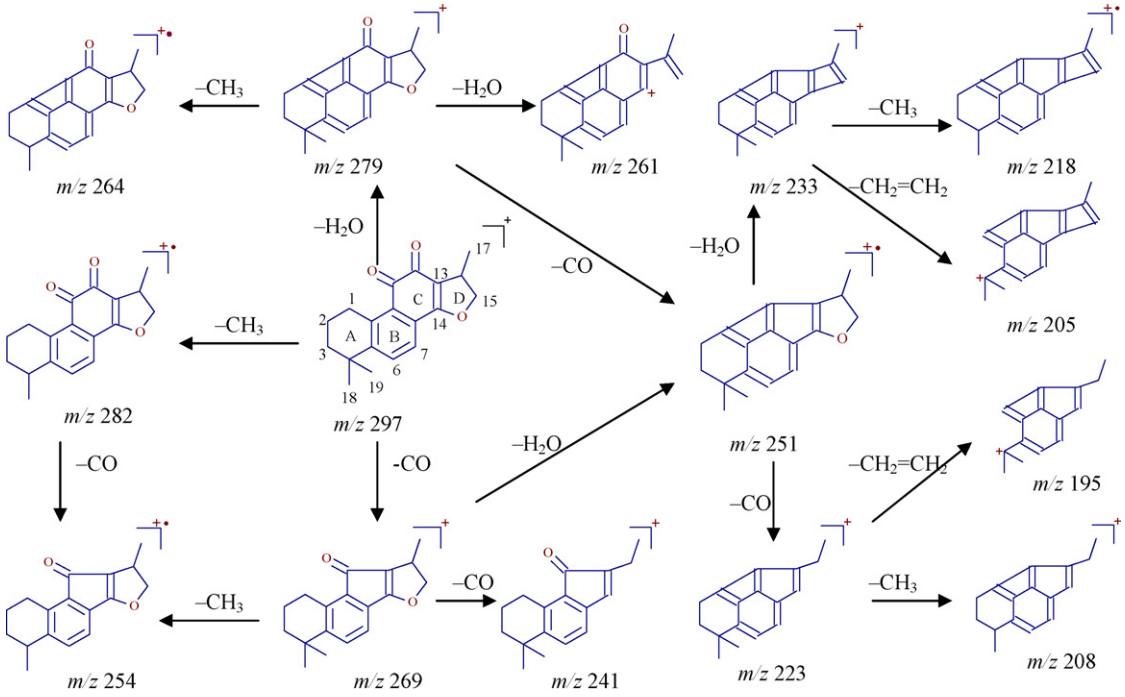

Fig. 3. The proposed fragmentation pathways of cryptotanshinone.

Table 1
Chromatographic retention time, mass spectrometric data and relative abundance of cryptotanshinone and its *in vivo* and *in vitro* phase I metabolites

Metabolites	Precursor ion	Retention time (min)	Data-dependent MS^n data (% base peak)	Relative abundance (%)
CT	$[M+H]^+$ 297	9.99	MS^2 [297]: 297(1), 282(15), 279(100), 269(2), 268(18), 254(25), 251(74), 237(7), 227(4), 209(3) MS^3 [297 → 279]: 279(7), 264(39), 261(34), 251(100), 237(58), 233(17), 223(21), 209(16), 197(14), 185(7) MS^3 [297 → 269]: 254(20), 251(68), 241(67), 227(100), 223(54) MS^4 [297 → 279 → 251]: 251(8), 236(41), 233(100), 223(47), 222(23), 209(22), 195(11), 183(11) MS^5 [297 → 279 → 251 → 233]: 218(36), 205(100) MS^5 [297 → 279 → 251 → 223]: 223(5), 208(100), 195(16), 194(20), 153(27)	56.3236
M1	$[M+H]^+$ 311	4.13	MS^2 [311]: 311(10), 296(64), 293(22), 283(69), 265(100), 251(6), 241(8), 237(13), 231(4) MS^3 [311 → 293]: 293(100), 275(37), 268(31), 265(90), 237(47), 225(71) MS^4 [311 → 293 → 275]: 247(100) MS^5 [311 → 293 → 275 → 247]: 219(100), 204(95)	0.2679
M2	$[M+H]^+$ 313	4.66	MS^2 [313]: 313(100), 295(95), 277(56), 267(68), 253(29), 249(37), 235(25), 229(18) MS^3 [313 → 295]: 295(56), 277(100), 249(51) MS^4 [313 → 295 → 277]: 259(64), 249(100)	0.4486
M3[a]	$[M+H]^+$ 329	5.38	MS^2 [329]: 311(71), 301(35), 297(54), 283(100), 267(44), 249(40), 226(34) MS^3 [329 → 311]: 293(92), 283(100), 278(77), 265(66) MS^3 [329 → 297]: 282(69), 269(100), 254(50) MS^3 [329 → 283]: 265(44), 255(100), 227(99), 209(41), 195(32) MS^4 [329 → 297 → 269]: 269(100), 254(81), 241(60)	0.0569
M4	$[M+H]^+$ 293	5.77	MS^2 [293]: 293(8), 278(17), 275(100), 265(11), 247(31), 229(4), 131(5) MS^3 [293 → 275]: 275(23), 260(9), 247(100), 219(9) MS^4 [293 → 275 → 247]: 232(26), 219(100), 204(63), 193(21), 191(21)	0.1389
M5	$[M+H]^+$ 313	6.30	MS^2 [313]: 313(86), 295(100), 277(93) MS^3 [313 → 295]: 277(100), 267(24), 253(23), 249(23), 239(16), 225(30) MS^4 [313 → 295 → 277]: 259(52), 249(30), 221(100)	0.1956
M6	$[M+H]^+$ 311	6.39	MS^2 [311]: 311(31), 293(82), 283(13), 275(100), 263(17), 253(31), 251(17), 249(11), 136(9) MS^3 [311 → 293]: 278(9), 275(100), 268(14), 251(50), 247(28) MS^4 [311 → 293 → 275]: 260(22), 247(100), 246(17) MS^5 [311 → 293 → 275 → 247]: 219(100)	0.3189
M7	$[M+H]^+$ 327	6.65	MS^2 [327]: 327(12), 312(86), 295(100), 247(12) MS^3 [327 → 295]: 295(100), 277(30), 267(9), 249(15) MS^4 [327 → 295 → 277]: 262(81), 259(81), 249(64), 231(100)	0.0293
M8	$[M+H]^+$ 309	6.86	MS^2 [309]: 309(100), 291(23), 281(95), 280(51), 277(17), 263(15), 249(8), 219(8), 171(6), 160(5) MS^3 [309 → 281]: 281(17), 263(100), 253(29), 235(15) MS^4 [309 → 281 → 263]: 248(32), 235(100), 219(41), 217(80)	0.0385
M9	$[M+H]^+$ 293	6.94	MS^2 [293]: 293(5), 278(9), 275(100), 265(7), 251(5), 247(21), 229(2) MS^3 [293 → 275]: 275(29), 260(6), 247(100), 229(4), 205(3) MS^4 [293 → 275 → 247]: 247(61), 232(15), 229(6), 219(100), 204(60), 193(14)	0.0321
M10	$[M+H]^+$ 287	7.03	MS^2 [287]: 287(1), 269(100), 263(1), 213(1) MS^3 [287 → 269]: 269(100), 254(25), 251(40), 241(74), 227(26), 213(38), 199(43), 183(7), 171(23) MS^4 [287 → 269 → 251]: 251(11), 236(100), 233(41), 223(80), 222(20), 209(63), 195(39), 181(42), 167(13), 153(16) MS^4 [287 → 269 → 241]: 226(36), 223(23), 213(74), 199(100), 197(63), 185(13), 171(42), 157(34), 155(12), 143(65) MS^5 [287 → 269 → 251 → 233]: 218(100), 205(54), 190(68) MS^5 [287 → 269 → 251 → 223]: 208(80), 195(100), 181(67)	0.0757
M11	$[M+H]^+$ 285	7.08	MS^2 [285]: 285(1), 267(100), 239(1), 211(1) MS^3 [285 → 267]: 267(14), 252(15), 249(14), 239(27), 225(29), 211(100), 197(10), 181(5), 169(3) MS^4 [285 → 267 → 239]: 221(70), 211(63), 197(100), 183(43) MS^4 [285 → 267 → 249]: 234(49), 231(32), 221(100), 207(25), 193(55), 179(17) MS^5 [285 → 267 → 239 → 211]: 196(54), 183(85), 181(100), 168(76) MS^5 [285 → 267 → 239 → 221]: 206(80), 193(100) MS^5 [285 → 267 → 249 → 221]: 206(100), 193(20), 191(21), 179(27), 178(67)	0.0415
M12	$[M+H]^+$ 339	7.28	MS^2 [339]: 339(1), 321(2), 311(6), 293(2), 279(100), 261(11) MS^3 [339 → 311]: 293(26), 281(32), 279(100), 261(68) MS^4 [339 → 311 → 293]: 265(100) MS^4 [339 → 311 → 279]: 261(100), 233(18) MS^5 [339 → 311 → 279 → 233]: 205(100)	0.0238
M13	$[M+H]^+$ 269	7.67	MS^2 [269]: 269(1), 251(100), 223(1), 213(1) MS^3 [269 → 251]: 251(7), 236(7), 233(24), 223(100), 207(27), 195(30), 192(4), 169(1) MS^4 [269 → 251 → 233]: 233(15), 218(55), 205(100), 190(13)	0.1003

Table 1 (Continued)

Metabolites	Precursor ion	Retention time (min)	Data-dependent MS^n data (% base peak)	Relative abundance (%)
			MS^4 [269 → 251 → 223]: 223(20), 208(22), 205(8), 195(100), 179(10)	
M14	$[M+H]^+$ 313	7.76	MS^2 [313]: 313(44), 295(100), 277(26), 271(42), 267(22), 253(40), 215(2), 200(33) MS^3 [313 → 295]: 295(32), 277(100), 267(37), 253(24), 249(51) MS^4 [313 → 295 → 277]: 277(15), 249(100), 235(16), 221(13)	0.3106
M15	$[M+H]^+$ 295	8.02	MS^2 [295]: 295(4), 280(15), 277(100), 267(18), 253(8), 249(52), 235(8), 225(31), 211(3), 185(2) MS^3 [295 → 277]: 277(45), 262(59), 249(100), 235(46), 231(18), 207(9) MS^3 [295 → 267]: 252(31), 249(67), 239(47), 225(100), 211(21), 197(23), 185(59) MS^4 [295 → 277 → 249]: 234(100), 221(94), 206(48), 195(9), 181(9), 165(10) MS^4 [295 → 267 → 239]: 211(76), 197(86), 185(100) MS^5 [295 → 277 → 249 → 221]: 221(16), 206(100), 193(15), 179(21)	13.9852
M16	$[M+H]^+$ 311	8.64	MS^2 [311]: 311(12), 293(81), 275(100), 269(17), 250(24), 247(16), 235(13), 229(8) MS^3 [311 → 293]: 275(100), 265(63), 247(38) MS^4 [311 → 293 → 275]: 247(100) MS^5 [311 → 293 → 275 → 247]: 219(100)	0.0102
M17	$[M+H]^+$ 267	9.90	MS^2 [267]: 267(82), 252(1), 249(1), 239(100), 217(3), 199(7), 185(45) MS^3 [267 → 239]: 224(3), 221(3), 211(4), 203(17), 185(7), 183(15), 171(100), 143(7) MS^3 [267 → 249]: 221(100) MS^4 [267 → 239 → 221]: 193(100) MS^4 [267 → 249 → 221]: 193(100)	0.0857
M18	$[M+H]^+$ 293	12.10	MS^2 [293]: 293(6), 278(11), 275(100), 265(7), 247(26), 230(3), 223(8), 222(3) MS^3 [293 → 275]: 275(18), 260(13), 247(100), 229(12) MS^4 [293 → 275 → 247]: 247(17), 232(23), 219(100), 204(47), 193(18), 191(10)	0.2351
M19	$[M+H]^+$ 295	14.51	MS^2 [295]: 295(57), 280(2), 277(100), 267(2), 253(4), 249(6), 235(3) MS^3 [295 → 277]: 277(4), 262(32), 249(100), 234(9), 231(11), 221(12), 206(3), 195(2), 179(1) MS^3 [295 → 267]: 252(14), 249(100), 239(26), 231(30), 225(19), 221(26) MS^4 [295 → 267 → 239]: 197(56), 179(100) MS^4 [295 → 277 → 249]: 234(86), 221(100), 206(38), 193(11), 143(5) MS^5 [295 → 277 → 249 → 221]: 221(10), 206(100), 193(27), 191(9), 167(12)	27.2818

[a] The metabolite was detected only *in vivo*.

Animals Center of Capital Medical University (CCMU). Rats were fasted for 8 h before use, but available to water ad libitum. Rat liver homogenate was prepared according to the literature [20]. Each incubation sample contained 3.75 mg/ml rat liver homogenate, 12.5 μg/ml cryptotanshinone and added to the volume of 400 ml by Krebs–Henseleit buffer (pH 7.4). The incubation samples without cryptotanshinone were used as blank control experiment. All the above operation was carried out on ice. After incubating in a shaking water bath for 4–6 h at 37 °C, the biotransformation was terminated by freezing at 4 °C. The samples were vortexed for 2 min and centrifuged at 3500 × *g* for 15 min. The supernatant were extracted 3 times by adding three-fold volume of ethyl acetate. Then the upper organic layers were collected and evaporated to dryness under a stream of nitrogen flow at 40 °C. The dried residues were redissolved in 200 μl of methanol followed by filtration with 0.22 μm for LC–DAD–ESI–MS^n analysis.

2.3. In vivo investigation

Male Sprague–Dawley rats (210–250 g) were fasted overnight but water was available ad libitum before use. The rats were anesthetized and fixed on a wooden plate. An abdominal incision was made and the rat bile duct was cannulated with PE-10 tube (i.d. 0.08 cm, Becton Dickinson, USA) for collection of the bile samples. Cryptotanshinone was dissolved in Tween-80 and normal saline to form the concentration of 2 mg/ml, before injection the drug solution was filtered by 0.22 μm filter. A single dose of 4 mg/kg cryptotanshinone was intravenously administered to rats by caudae vein and the same concentration of Tween-80 was administered for blank control. A heating-lamp was used for maintaining the body temperatures during the experimental procedures. Bile samples were collected for 12 h and all the samples were stored at −80 °C until extraction and analysis. The bile samples were extracted and operated as Section 2.2.

2.4. Instrumentation and analytical condition

The LC–ESI–MS system consisted of a HPLC system (Series 1100, Agilent Technology, Palo Alto, CA, USA) including a HP-1100 binary pump, a vacuum degasser and an auto-sampler and coupled to Finngian LCQ Deca XP ion trap mass spectrometer (ITMS) equipped with an electrospray source (ESI) (Thermo Finnigan, San Jose, CA, USA) and a diode array detector (DAD) (Agilent Technologies, Palo Alto, CA, USA). The LC–ESI–MS system was controlled by Xcalibur® (version 1.3) software.

Separations of the metabolites were achieved on a Betamax Acid C_{18} reversed-phase LC column (150 mm × 2.1 mm i.d., 5 μm; Thermo Electron, CA, USA) at a flow rate of 0.2 ml/min at ambient temperature. The mobile phase was composed of methanol and water (75:25 v/v) and a volume of 5 μl of sample was always introduced into the LC–ESI–MS system. The run time of samples in all instances totaled 20 min. The effluent from the chromatographic column was monitored by UV detection at 254 nm and DAD spectra were acquired every 0.5 s. The flow from the UV detector (unsplit) was directed into the mass spectrometer with a minimal amount of PEEK tube (Upchurch, Oak Harbor, WA, USA). The experiments utilized electrospray ionization in positive ion and/or negative ion mode.

The ESI–MS was operated at the sheath flow rate of 60 psi; capillary temperature of 350 °C; capillary voltage of 12 V and elec-

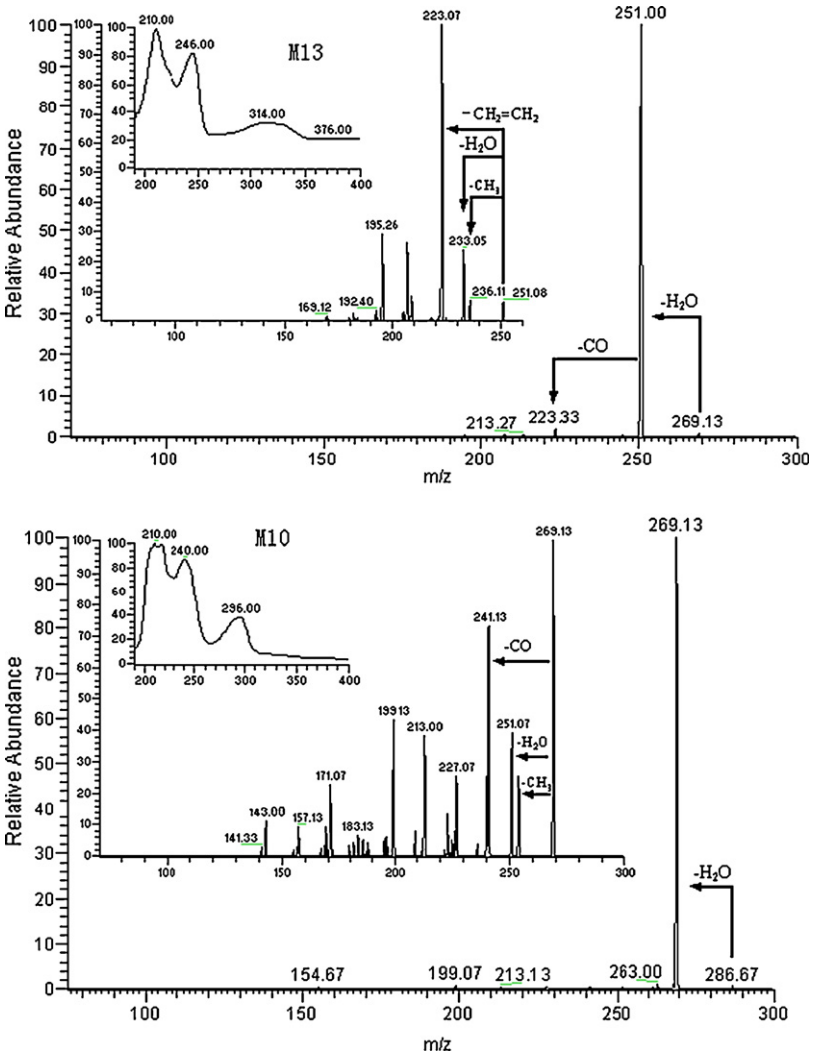

Fig. 4. MS^n (n = 2–3) spectra and UV spectra of M10 and M13. (M10: MS^2 [287], MS^3 [287 → 269] spectra and UV spectrum of M10; M13: MS^2 [269], MS^3 [269 → 251] spectra and UV spectrum of M13.)

trospray voltage ranged from +3.5 to +5 kV. Ultra-high purity helium was used as collision gas for the collision induced dissociation (CID) experiments. Nitrogen was used for both drying gas and nebulizing gas, which was set at 25 and 5 psi of sheath and auxiliary gas, respectively. The MS^n product ion spectra were produced by collision induced dissociation of the protonated molecule $[M+H]^+$ ion of each analyte at their respective HPLC retention times. Collision energy for the metabolites was dependent on different metabolites from 30 to 40% with isolation width of 1.0 Da and activation time of 30 ms. The effluent from the column was on-line transferred to ESI–MS system without splitting. In a separate analysis, the data-dependent MS/MS scanning feature of the ion trap was used to ensure comprehensive MS/MS information of the metabolites. The ion spay interface and mass spectrometric parameters were optimized to obtain maximum sensitivity at the unit resolution.

3. Results and discussion

Owing to the development of soft ionization techniques, mass spectrometry has assumed an increasingly important role in pharmaceutical and biomedicine. ESI–MS, a versatile technique, is applied in all stages of drug development including chemical synthesis, drug target identification, library verification, drug analysis and toxicology, especially in drug metabolism and pharmacokinetics [21,22]. While different combinations of liquid chromatography with IR, UV/DAD, and NMR are widely applied, they are extensively employed in conjunction with MS techniques. Hyphenated MS techniques are frequently the initial choice for drug metabolite detection and identification because of their sensitivity and convenience compared with other methods [23–26].

The first step in this work involved the characterization of the ultraviolet spectral and mass spectral properties of the parent drug. Full scan mass spectral analyses of cryptotanshinone showed a protonated molecule ion of m/z 297. Extracted ion chromatograms of cryptotanshinone and its phase I and phase II metabolites in rat are presented in Fig. 1. CID analyses of these pseudo-molecular ions yielded the mass spectra are presented in Fig. 2. The suggested fragmentation patterns of cryptotanshinone are presented in Fig. 3. The mass spectral patterns of cryptotanshinone served as templates in the elucidation of the structures of the proposed metabolites. Structural determination of metabolites was facilitated by the fact that the parent compound undergoes extensive and well definable fragmentation under MS/MS conditions. In order to reduce the endogenous interference, rat hepatic

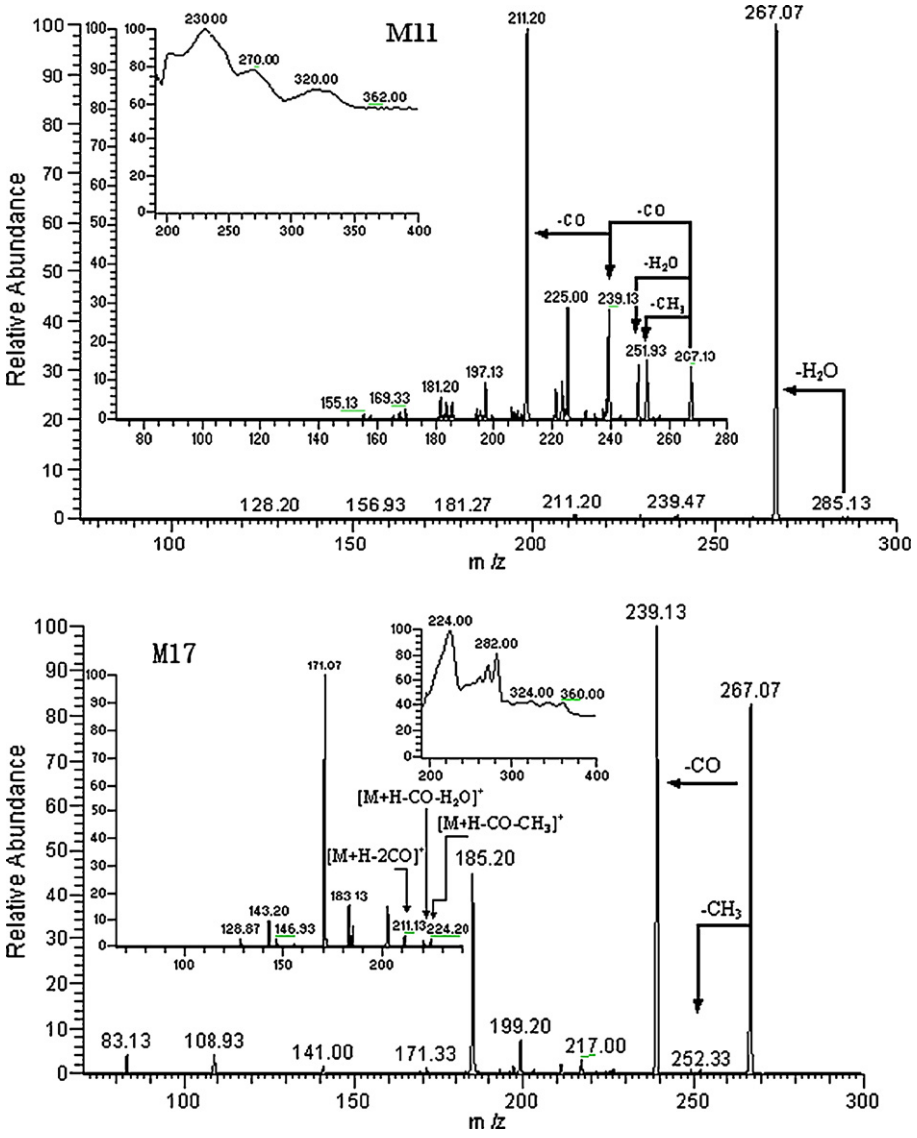

Fig. 5. MS^2, MS^3 spectra and UV spectra of M11 and M17. (M11: MS^2 [285], MS^3 [285 → 267] spectra and UV spectrum of M11; M17: MS^2 [267], MS^3 [267 → 239] spectra and UV spectrum of M17.)

homogenate samples and bile samples were extracted with ethyl acetate.

The investigation involved the characterization of the ultraviolet spectral and the mass spectral properties of the parent drug and its metabolites. The full scan mass spectra of metabolite samples were compared with that of the blank and the parent drug to find the proposed metabolites. These compounds were analyzed by LC–MS^n. Retention times, ultraviolet spectra, changes in observed mass (ΔM) and spectral patterns of product ions of metabolites were compared with that of cryptotanshinone to identify metabolites and elucidate their structures.

After determination of the retention time, the ultraviolet spectra and the mass spectra of the proposed metabolite molecules, the retention time dependent MS/MS scans were programmed to acquire CID data on-line. Complete structural identification of metabolites may be hindered by the absence of useful product ions in the MS or MS/MS spectrum, thus, the pseudo MS^n mass spectra, via in-source fragmentation of molecular ions, were used for more precise structural identification of metabolites. We could reveal the essential change in many product ions of metabolites and elucidate the structures of metabolites via a series comparison of the product ions of the metabolites with that of the parent drug. Based on the method described above, we found 25 extracted ion chromatographic peaks which were the proposed phase I and phase II metabolites (M1–M25) *in vivo* and *in vitro*. The parent ion, major metabolite product ions and relative abundant of content along with their HPLC retention times of 19 metabolites both *in vivo* and *in vitro* are summarized in Table 1. The major metabolic pathways of cryptotanshinone in rat were dehydrogenation, hydroxylation, D-ring cleavage and hydrolysis or oxidation in phase I reaction, *O*-glucuronidation and *O*-sulfatation in phase II reaction.

3.1. *In vitro metabolites of cryptotanshinone*

3.1.1. *Group I: mass fragmental patterns of parent drug*

CT was observed as its protonated molecule $[M+H]^+$ at m/z 297 with a retention time of 9.99 min comparing with the standard compound. The MS^n ($n = 2–5$) spectra gave prominent ions at m/z 282, 279, 269, 254, 251, 241, 223, 233, 218, 208, 205 and 195. The retention time, UV spectrum and the MS^n spectra were the same as those of CT. Therefore, this compound was confirmed as cryptotanshinone, the unchanged parent drug. The product ions spectra and

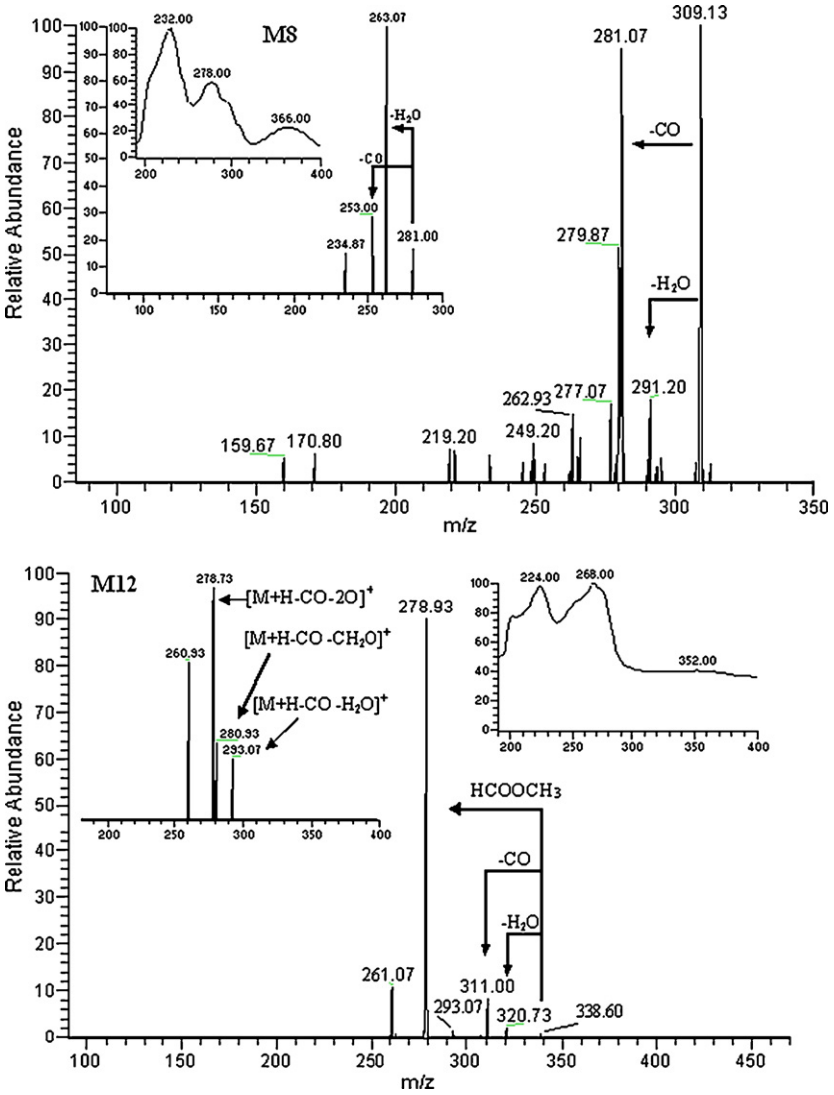

Fig. 6. MS^2, MS^3 spectra and UV spectra of M8 and M12. (M8: MS^2 [309], MS^3 [309 → 281] spectra and UV spectrum of M8; M12: MS^2 [339], MS^3 [339 → 311] spectra and UV spectrum of M12.)

UV spectrum of the protonated molecule of CT are shown in Fig. 2. The $[M+H]^+$ ion at *m/z* 297 formed a prominent product ion at *m/z* 279 ($[M+H-H_2O]^+$) when a collision energy of 40% was used. The ion at *m/z* 279 was further subjected to MS^3 analysis and produced an ion at *m/z* 251 ($[M+H-H_2O-CO]^+$), which further yielded the ions at *m/z* 233 ($[M+H-2H_2O-CO]^+$) and 223 ($[M+H-H_2O-2CO]^+$) as the base peak in the MS^4 spectrum. The ion at *m/z* 233 further fragmented to form ions at *m/z* 218 and 205 via losses of CH_3 and $CH_2{=}CH_2$, respectively. The ion at *m/z* 223 further fragmented to form ions at *m/z* 208 and 195 through loss of CH_3 and $CH_2{=}CH_2$, respectively. Losses of CH_3 also appeared in the MS^n ($n = 2$–4) spectra (*m/z* 297 → 282, 279 → 264, 269 → 254, 251 → 236). The proposed fragmentation pathway of CT is illustrated in Fig. 3. The fragmentation mechanism of CT could help to elucidate and identify the metabolite structures of cryptotanshinone.

3.1.2. Group II: dehydrogenated metabolites (M15, M19; M4, M9 and M18)

M15 and M19, eluted at 8.02 and 14.51 min, respectively, both gave rise to protonated molecules $[M+H]^+$ at *m/z* 295.The MS^n characteristic ions of M15 and M19 (*m/z* 280, 277, 267, 249, 239, 221, 206 and 193) are 2 Da less than that of cryptotanshinone. The retention time, the MS^n spectra and the UV spectra of M19 were the same as those of tanshinone IIA. Therefore, M19 was confirmed as tanshinone IIA, which was the major metabolite of cryptoanshinone by the dehydrogenated reaction. The MS^n product ions spectra of M15 were similar with M19 (seen in Table 1), but the UV spectrum ($\lambda_{max} = 260$ nm) was different, according to the literature [27–29], M15 was characterized as the 1,2-dehydrocryptotanshinone or 2,3-dehydrocryptotanshinone.

M4, M9 and M18, eluted at 5.77, 6.94 and 12.10 min, respectively, all they gave rise to protonated molecules $[M+H]^+$ at *m/z* 293 and 2 Da less than that of tanshinone IIA. Their MS^n spectra were almost identical. The main product ions of M4, M9 and M18 are shown in Table 1. Their characteristic fragmentation pathways are similar: *m/z* 293 → 275 → 247 → 219 → 204, 191, via losses of H_2O, CO, CH_3 or $CH_2{=}CH_2$. Losses of CH_3 (*m/z* 293 → 278, 275 → 260, 247 → 232) were also observed in the MS^n ($n = 2$–4) spectra. All the main fragment ions of them were 2 Da less than those of tanshinone IIA. Therefore, M4, M9 and M18 were tentatively proposed as the dehydrogenated metabolites of tanshinone IIA. According to the literature [27–30], M4 and M9 were identified as 1,2-dehydrotanshinone IIA or 2,3-dehydrotanshinone IIA; M18 was identified as 1,3-dehydrotanshinone IIA.

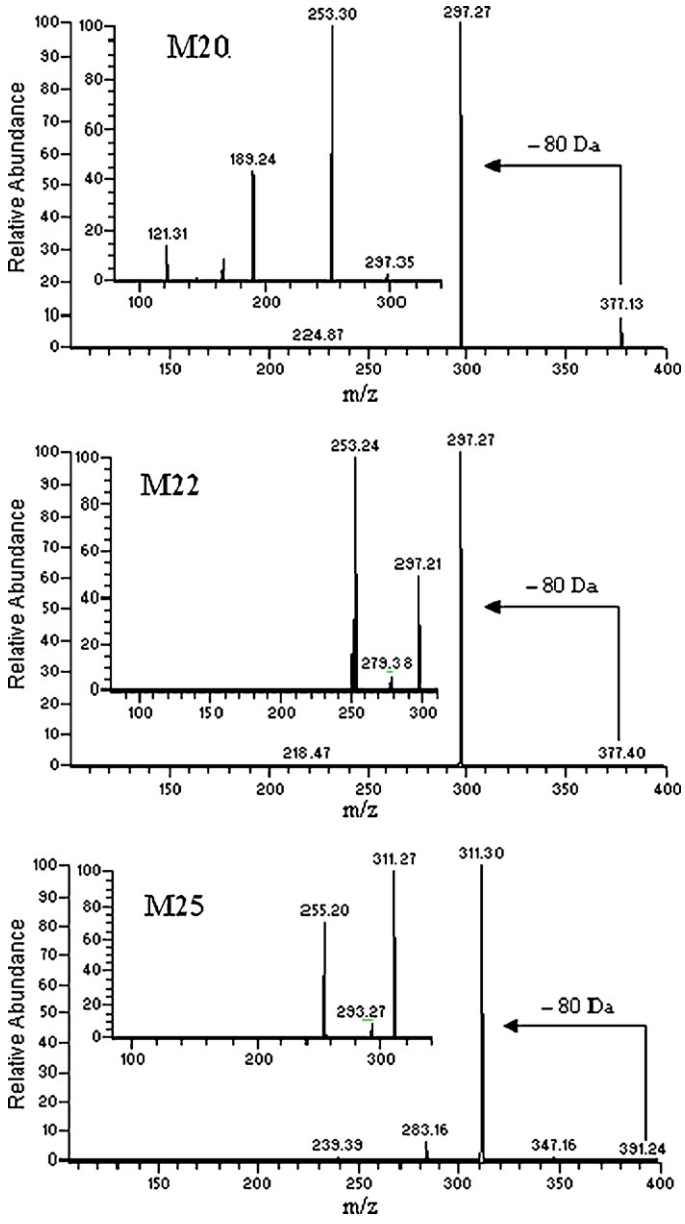

Fig. 7. MS/MS and MS^3 spectra of M20, M22 and M25 of cryptotanshinone.

3.1.3. Group III: metabolites of furan ring cleavage (M13, M10, M17 and M11)

M13, eluted at 7.67 min, gave $[M+H]^+$ at *m/z* 269. The MS^n (*n* = 2–4) spectra gave prominent ions at *m/z* 251, 233, 223, 218, 208, 205 and 195 (shown in Table 1), which were similar to that of cryptotanshinone. M13 was 28 Da less than that of cryptotanshinone, but the UV spectra between them were different, so there could be some change in their structures. When a collision energy of 35% was used, the $[M+H]^+$ at *m/z* 269 of M13 produced a prominent ion at *m/z* 251, resulting from the loss of H_2O, which in MS^3 analysis underwent losses of CH_3, H_2O and CH_2=CH_2 to generate ions at *m/z* 236, 233 and 223, respectively. The *m/z* 233 ion obtained then produced ions at *m/z* 218 and 205 in the same pathway as cryptotanshinone. The ion at *m/z* 223 underwent MS^4 analysis and produced ions at *m/z* 208, 205 and 195, via losses of CH_3, H_2O and CO, respectively. The product ions spectra and the UV spectrum of M13 are shown in Fig. 4. According to the analysis above, M13 was elucidated as the metabolite by cleavage of furan ring and loss of CO from furan ring of cryptotanshinone.

M10 was observed as its protonated molecule $[M+H]^+$ at *m/z* 287 with a retention time of 7.03 min. A prominent ion at *m/z* 269 ($[M+H-18]^+$) was observed in the MS/MS spectrum (shown in Fig. 4), resulting from the loss of H_2O. The fragmentation mechanisms of MS^3 [*m/z* 269], MS^4 [*m/z* 251] and [*m/z* 241] were similar, via losses of CH_3, H_2O, CO and 42 Da (CH_2=$CHCH_3$) to form their daughter ions. The fragmentation pathways of MS^5 [*m/z* 233] and [*m/z* 223] were the same as those of MS^5 [*m/z* 233] and [*m/z* 223] of cryptotanshinone, respectively. The characteristic mechanism of M10 was similar to that of M13. Therefore, M10 was tentatively elucidated as the hydroxyl metabolite of M13 at the C-14 position in C-ring or the hydroxylated metabolite of M13 at the side chain hydrocarbon C-16 position in C-ring. The major product ions of M10 from MS^n (*n* = 2–5) spectra are shown in Table 1.

M17 gave rise to protonated molecule $[M+H]^+$ at *m/z* 267, with a retention time of 9.90 min, and 28 Da less than that of tanshinone IIA. The MS/MS spectra of M17 from the $[M+H]^+$ ion at *m/z* 267 gave a prominent $[M+H-28]^+$ ion at *m/z* 239 and minor ions at *m/z* 252 ($[M+H-15]^+$), 249 ($[M+H-18]^+$) (shown in Fig. 5). The MS^3 spectra of *m/z* 239 and 249 yielded the ion at *m/z* 221 as the base peak, corresponding to losses of H_2O and CO, respectively. Losses of CH_3 and CO to form the ions at *m/z* 224 and 211, respectively, were observed in MS^3 spectrum of *m/z* 239. The MS^4 spectrum of *m/z* 221 yielded ion at *m/z* 193, corresponding to loss of CH_2=CH_2 in the same pathway as tanshinone IIA. According to the analysis above, M17 was tentatively elucidated as the metabolite of tanshinone IIA by cleavage of furan ring and loss of CO from furan ring.

M11, eluted at 7.08 min, gave rise to protonated molecule $[M+H]^+$ at *m/z* 285. Fragmentation of the $[M+H]^+$ ion at *m/z* 285 involved initial loss of H_2O (seen in Fig. 5). Then the product ion obtained at *m/z* 267 underwent similar fragmentation to the ions from M17 (*m/z* 267 → 239 → 221 → 193, 267 → 249 → 221 → 193). The major product ions of M11 are shown in Table 1. Besides ion at *m/z* 221, the ion at *m/z* 239 could further fragmented to form ion at *m/z* 211, which in MS^5 analysis underwent losses of CH_3 and CH_2=CH_2 to generate ions at *m/z* 196 and 183, respectively. The ion at *m/z* 249 underwent MS^4 analysis and produced ions at *m/z* 234, 231 and 221 via losses of CH_3, H_2O and CO, respectively. The losses of CH_3 (*m/z* 267 → 252, 221 → 206) were also observed in the MS^3 and MS^5 spectra. According to the analysis above, M11 was tentatively elucidated as the hydroxylated metabolite of M17 at the side chain hydrocarbon C-16 position in C-ring.

3.1.4. Group IV: M8 (tanshinaldehyde) and M12 (methyl tanshinonate)

M8 was observed as a protonated molecule $[M+H]^+$ at *m/z* 309, with a retention time of 6.86 min. In MS^n (*n* = 2–4) spectra, the characteristic ions of M8 at *m/z* 291 ($[M+H-H_2O]^+$), 281 ($[M+H-CO]^+$), 263 ($[M+H-CO-H_2O]^+$), 253 ($[M+H-2CO]^+$), 248 ($[M+H-CO-H_2O-CH_3]^+$) and 235 ($[M+H-H_2O-2CO]^+$) were observed (Table 1). In addition, an ion at *m/z* 280 was observed in the MS/MS spectrum (shown in Fig. 6) which attributed to the loss of 29 Da (CHO); it indicated that the structure of M8 had an aldehyde group. According to the literature [27,28], M8 was characterized as tanshinaldehyde, a metabolite of tanshinone IIA at A-ring C-4 methyl oxidation. The UV spectrum and the fragmentation of M8 were slightly different from that of tanshinone IIA owing to the methyl groups at C-4 in tanshinone IIA had been converted into aldehyde group. Tanshinaldehyde also existed in the roots of *S. miltiorrhiza* Bunge [19].

M12, eluted at 7.28 min, gave rise to protonated molecule $[M+H]^+$ at *m/z* 339. A prominent ion at *m/z* 279 ($[M+H-60]^+$) was observed in the MS/MS spectrum (seen in Fig. 6), resulting from the

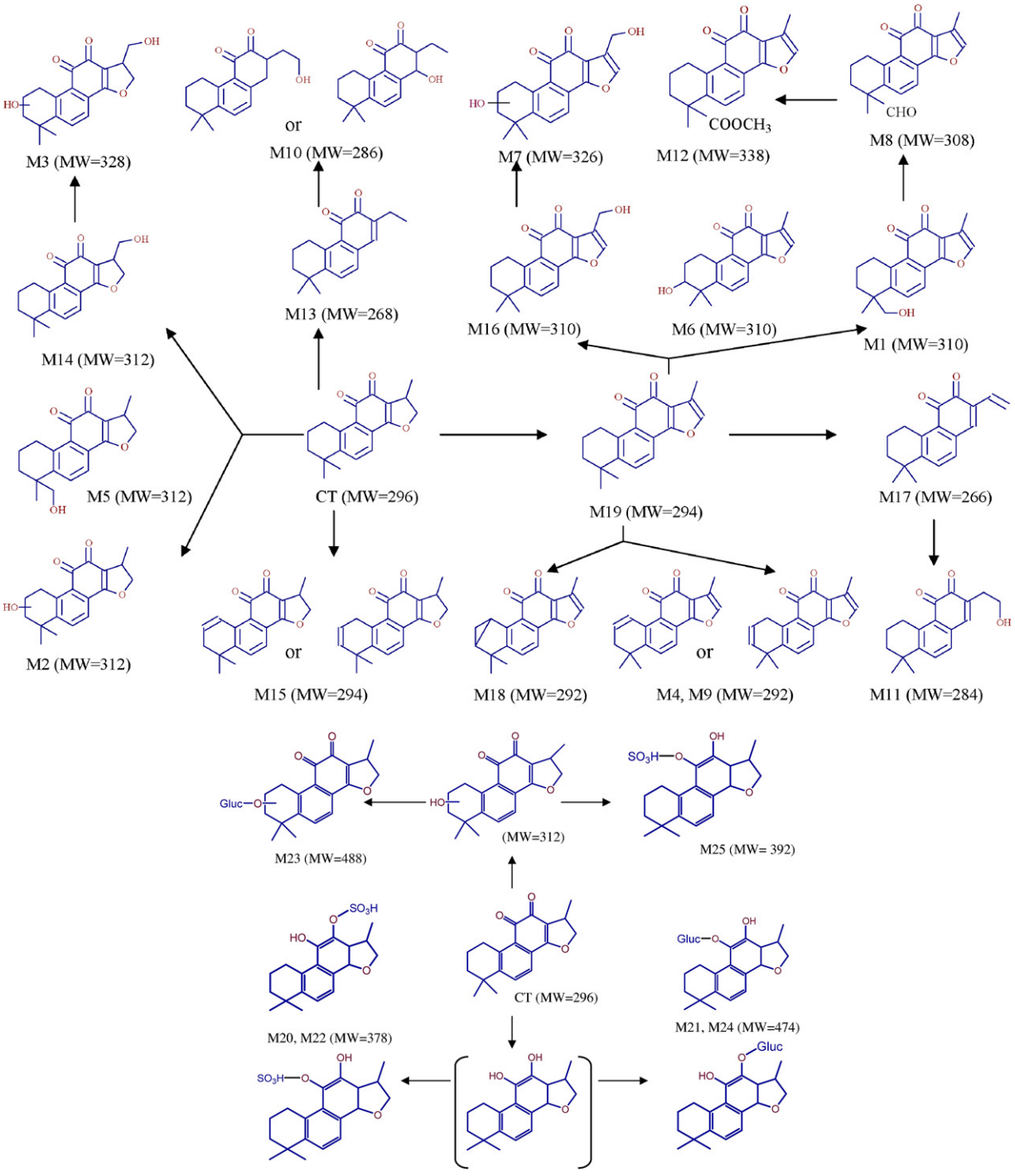

Fig. 8. Proposed biotransformation pathways of cryptotanshinone in rats.

loss of 60 Da ($HCOOCH_3$). The minor ions at m/z 321($[M+H-18]^+$), 311 ($[M+H-28]^+$), 293 ($[M+H-46]^+$) were attributed to successive losses of H_2O and CO. The ion at m/z 279 was subjected to MS^4 analysis and product ions at m/z 233 and 261 via losses of 46 Da (–H_2O, –CO) and H_2O, respectively. The other two ions at m/z 265 and 205 were attributed to loss of 28 Da (CO) from m/z 293 and 233, respectively. Therefore, M12 was designated as methyl tanshinonate, a metabolite of tanshinaldehyde from aldehyde oxidation at C-4 side chain. The UV spectrum and the fragmentation of M12 were somewhat different from that of tanshinone IIA owing to –CH_3 group at C-4 of tanshinone IIA oxidized to form –$COOCH_3$.

3.1.5. Group V: monohydroxylated (M2, M5, M14, M1, M6 and M16) and dihydroxylated (M3 and M7) metabolites

M2, M5 and M14 eluted at 4.66, 6.30 and 7.76 min, respectively, all gave the quasi-molecular ion of m/z 313, and 16 Da higher than that of cryptotanshinone. An obvious $[M+H-18]^+$ ion at m/z 295, formed by loss of H_2O, was observed in the MS/MS spectrum. Their major product ions are shown in Table 1. The characteristic fragmentation mechanisms of them are similar: m/z 313 → 295 → 277 → 249 → 221. According to the MS^n spectra, retention time, and polarity of the metabolite with one hydroxyl group of cryptotanshinone [16,30], M2, M5 and M14

were elucidated as A-ring hydroxycryptotanshinone, 18-methyl hydroxycryptotanshinone and 17-methyl hydroxylcryptotanshinone, respectively.

M1, M6 and M16 eluted at 4.13, 6.39 and 8.64 min, respectively, all gave rise to protonated molecules $[M+H]^+$ at m/z 311 and were 16 Da higher than that of tanshinone IIA. The major product ions of M1, M6 and M16 are shown in Table 1. The characteristic mechanism pathways of them are similar: m/z $311 \rightarrow 293 \rightarrow 275 \rightarrow 247 \rightarrow 219 \rightarrow 204$, through losses of H_2O, CO or CH_3. According to the retention time, MS^n ($n = 2$–5) spectra and the polarity of hydroxytanshinone IIA [16,27], M1, M6 and M16 were identified as tanshinone IIB, 3-hydroxytanshinone IIA and przewaquinone A, respectively.

M7 was observed as protonated molecule $[M+H]^+$ at m/z 327 with a retention time of 6.65 min. M7 was 32 Da higher than that of tanshinone IIA and 16 Da higher than that of hydroxyl metabolites of tanshinone IIA. The MS^3 [327 → 295] spectrum produced ions at m/z 295, 277, 267, 249 and 231 in the same pathway as that of tanshinone IIA. Therefore, M7 was tentatively proposed to be the dihydroxytanshinone IIA, one hydroxylation position occurs at C-17 or C-18 methyl group, and the other hydroxylation occurs at A-ring.

3.2. *In vivo* metabolites of cryptotanshinone

Taking the results of *in vitro* incubation as reference, *in vivo* metabolism of cryptotanshinone was studied after a single dose intravenous administration. Bile was collected and extracted with ethyl acetate. Then the upper organic layers were evaporated to dryness and the reconstitutes were analyzed by LC–ESI–MS^n in positive ion modes. The aqueous layers were treated with methanol for protein precipitation and the supernatant were evaporated to dryness, the reconstitutes were analyzed by LC–ESI–MS in negative ion mode. In the organic layer, trace amounts of phase I metabolites were observed (shown in Fig. 1), most of phase I metabolites were elucidated and identified *in vitro* incubation except M3. *O*-Glucuronidated and *O*-sulfated metabolites were detected by ESI–MS in the negative ion mode in aqueous layer. Neutral loss scan in MS/MS mode was used to screen the proposed phase II metabolites such as glucuronidated product with 176 Da and sulfated product with 80 Da. The detected conjugated metabolites were confirmed by LC–MS and MS/MS analysis. Based on the above method, six phase II metabolites were observed, the extracted mass chromatograms of them (M20–M25) are shown in Fig. 1.

Phase I metabolite M3 was observed as protonated molecule $[M+H]^+$ at m/z 329 with a retention time of 5.38 min and was 32 Da high than that of cryptotanshinone. The MS^3 [329 → 297] and MS^4 [329 → 297 → 269] spectra gave the characteristic ions at m/z 297, 282, 269, 254 and 241 in the same pathway as that of cryptotanshinone. Therefore, M3 was tentatively proposed to be the dihydroxycryptotanshinone (seen in Fig. 8).

M20 and M22 were observed as sulfated metabolites with retention times of 3.00 and 5.36 min. They were detected with the $[M-H]^-$ ion at m/z 377, which MS/MS spectrum showed an intense ion at m/z 297 corresponding to the neutral loss of 80 Da (seen in Fig. 7). Their retention time and the MS^3 spectra have slight difference. According to the MS data and the literature [31], tanshinone IIA could be firstly reduced to tanshinone IIA catechol and then formed to the position isomers of catechol conjugates. Thus, M20 and M22 might be cryptotanshinone catechol sulfate conjugates which could be position isomers. Similarly, the detections of the metabolites M21 and M24 ($[M-H]^- = 473$) from the observation of the neutral loss of 176 Da were related to cryptotanshinone catechol glucuronidation conjugates which could be position isomers, and the results were confirmed by the MS/MS analysis.

Another sulfated metabolite M25 was detected at 6.49 min with the neutral loss scan of 80 Da in the negative ion mode. The obtained $[M-H]^-$ ion at m/z 391 indicated that hydroxylated and sulfated metabolite of cryptotanshinone was existed. The MS/MS spectrum of M25 showed a prominent ion at m/z 311 corresponding to the neutral loss of 80 Da, which underwent MS^3 analysis and produced ions at m/z 293 and 255 (shown in Fig. 7). Similarly, the detection of the glucuronidated metabolites M23 ($[M-H]^- = 487$) from the observation of the neutral loss of 176 Da was related to the hydroxylated metabolites of cryptotanshinone and confirmed by the MS/MS analysis.

4. Conclusion

This investigation described the application of LC–DAD–MS method with diode array detection and electrospray ionization mass spectra, positive ion and/or negative ion mode and collision induced dissociation to elucidate and identify the *in vitro* and *in vivo* metabolites of cryptotanshinone. Nineteen phase I metabolites and six phase II metabolites of cryptotanshinone were observed. The structures and fragment pathways of the metabolites were elucidated and analyzed (shown in Fig. 8). The structural analysis indicated that the *in vivo* and *in vitro* phase I metabolites of cryptotanshinone can be mainly divided into four categories: dehydrogenation, hydroxylation, furan ring cleavage and side chain oxidation. Among these metabolic reactions, the dehydrogenation was the predominant pathway and the dehydrogenated metabolites of cryptotanshinone were the predominant metabolites. *O*-Glucuronidation and *O*-sulfation metabolites of cryptotanshinone were the major phase II metabolic pathways. This investigation contributes to new information on cryptotanshinone metabolic mechanism and development of a novel drug which is essential for understanding the safety and efficacy.

Acknowledgements

The authors thank the National Foundation of Natural Sciences of China (No. 30472057), Beijing Natural Science Foundation Program (No. 7052007) and Scientific Program of Beijing Municipal Commission of Education (No. KM200410025003) for their financial supporting.

References

[1] T.H. Xue, R. Roy, Science 300 (2003) 740–741.
[2] J. Sun, S.H. Huang, B.K. Tan, M. Whiteman, Y.C. Zhu, Y.J. Wu, Y. Ng, W. Duan, Y.Z. Zhu, Life Sci. 76 (2005) 2849–2860.
[3] J. Ye, H. Duan, X. Yang, W. Yan, X. Zheng, Planta Med. 67 (2001) 766–767.
[4] M. Xue, Y. Cui, H.Q. Wang, Y.B. Shi, B. Zhang, Y.J. Luo, Z.T. Zhou, W.J. Xia, R.C. Zhao, Chin. J. Vet. Drug 33 (1999) 15–18.
[5] Y.G. Gao, Y.M. Song, Y.Y. Yang, W.F. Liu, J.X. Tang, Acta Pharmacol. Sin. 14 (1979) 75–82.
[6] E.H. Cao, X.Q. Liu, J.F. Li, Acta Biophys. Sin. 12 (1996) 339–343.
[7] X.M. Hu, M.M. Zhou, M.X. Hu, J. Wang, F.D. Zeng, Chin. Pharmacol. Bull. 22 (2006) 436–440.
[8] M.A. Mosaddik, Phytomedicine 10 (2003) 682–685.
[9] Z. Zhou, S.Q. Wang, Y. Liu, A.D. Miao, Biochim. Biophys. Acta 1760 (2006) 1–9.
[10] Q.T. Yuan, Y.B. Deng, X.G. Liu, J. Hu, S.N. Li, Z.G. Liu, Chin. J. Pathophysiol. 21 (2005) 993–996.
[11] H.B. Li, F. Chen, J. Chromatogr. A 925 (2001) 109–114.
[12] X.L. Li, X.R. Li, L.J. Wang, Y.H. Li, Y.X. Xu, M. Xue, J. Pharm. Biomed. Anal. 44 (2007) 1106–1112.
[13] M. Xue, Y. Cui, H.Q. Wang, Z.H.Y. Hu, B. Zhang, J. Pharm. Biomed. Anal. 21 (1999) 207–213.
[14] M.Z. Xie, Z.H.F. Shen, Acta Pharmceut. Sin. 18 (1983) 90–96.

[15] M. Xue, Y. Cui, H.Q. Wang, B. Zhang, Y.J. Luo, Asian J. Drug Metab. Pharmacokinet. 24 (2002) 271–276.
[16] J.H. Sun, M. Yang, J. Han, B.R. Wang, X.C.H. Ma, M. Xu, P. Liu, D.A. Guo, Rapid Commun. Mass Spectrom. 21 (2007) 2211–2226.
[17] P. Li, G.J. Wang, J. Li, H.P. Hao, Ch.N. Zheng, J. Chromatogr. A 1104 (2006) 366–369.
[18] P. Li, G.J. Wang, J. Li, H.P. Hao, Ch.N. Zheng, J. Mass Spectrom. 41 (2006) 670–684.
[19] M. Xue, Y.B. Shi, Y. Cui, B. Zhang, Y.J. Luo, Z.T. Zhou, W.J. Xia, R.C. Zhao, H.Q. Wang, Nat. Product Res. Develop. 12 (2000) 27–32.
[20] J.A.C. Bierman, H. Lingeman, H.J.E.M. Reeuwijk, E.A. De Bruijn, U.R. Tjaden, J.V.D. Greef, J. Pharm. Biomed. Anal. 7 (1989) 611–617.
[21] L.L. Lee, M.L. Herold, A.G. Zacchei, J. Chromatogr. B 685 (1996) 323–328.
[22] A. Cailleux, A. LeBouil, B. Auger, G. Bonsergent, A. Turcant, P. Allain, J. Anal. Toxicol. 23 (1999) 620–624.
[23] N.J. Bailey, P.D. Stanley, S.T. Hadfield, J.C. Lindon, J.K. Nicholson, Rapid Commun. Mass Spectrom. 14 (2000) 679–684.
[24] W.H. Schaefer, J. Politowski, B. Hwang, F. Dixon Jr., A. Goalwin, L. Gutzait, K. Anderson, C. DeBrosse, M. Bean, G.R. Rhodes, Drug Metab. Dispos. 26 (1998) 958–969.
[25] X. Yu, D.H. Cui, M.R. Davis, J. Am. Soc. Mass Spectrom. 10 (1999) 175–183.
[26] L.L. Lopez, X. Yu, D. Cui, M.R. Davis, Rapid Commun. Mass Spectrom. 12 (1998) 1756–1760.
[27] H.J. Sun, M. Yang, X.M. Wang, M. Xu, A.H. Liu, D.A. Guo, J. Pharm. Biomed. Anal. 44 (2007) 564–574.
[28] H.J. Sun, M. Yang, J. Han, B.R. Wang, X.C. Ma, M. Xu, P. Liu, D.A. Guo, Rapid Commun. Mass Spectrom. 21 (2007) 1266–1280.
[29] J. Liu, J.L. Wu, X.R. Wang, Z.W. Cai, Rapid Commun. Mass Spectrom. 21 (2007) 2992–2998.
[30] M. Yang, A.H. Liu, S.H.H. Guan, J.H. Sun, M. Xu, D.A. Guo, Rapid Commun. Mass Spectrom. 20 (2006) 1266–1280.
[31] H.P. Hao, G.J. Wang, N. Cui, J. Li, L. Xie, Z.Q. Ding, Curr. Drug Metab. 8 (2007) 137–149.